ELSEVIER

Biochimica et Biophysica Acta 1228 (1995) 73–85

BBA Biochimica et Biophysica Acta

Optically-detected magnetic field effects on the D1-D2-cyt *b*-559 complex of Photosystem II. Temperature dependence of kinetics and structure

Robert van der Vos, Arnold J. Hoff *

Department of Biophysics, Huygens Laboratory, Leiden University, P.O. Box 9504, 2300 RA Leiden, The Netherlands

Received 30 May 1994; accepted 9 November 1994

Abstract

The magnetic field effect (MFE) on photosynthetic reactions in the D1-D2 reaction centre complex was studied using a new field modulation technique, and monitoring the absorbance from 1.2 to 200 K. The MFE recorded at low temperature (below 60 K) showed several features that cannot be due to the intrinsic properties of the primary donor triplet only. The temperature dependence of the amplitude of the MFE was simulated using a thermally activated charge-recombination rate from the radical-pair singlet state to the ground state and thermally activated charge recombination to the excited primary donor state. Due to repeated re-population of the excited state at high temperatures, triplet formation by intersystem crossing becomes important. The simulation yields upper limits for the activation energies of the two recombination processes of 26 meV and 70 meV for recombination to the singlet ground and excited state, respectively. From a Gaussian deconvolution of magnetic field-induced Triplet-minus-Singlet (T − S) spectra recorded at different temperatures in the range of 1.2 to 200 K, it is concluded that the conformation of one of the main components of the T − S spectra is transformed between 50 K and 70 K. Furthermore, going on to higher temperatures, an additional bleaching appears centered at 674.5 nm. The additional component could be due to delocalisation of the primary donor triplet. In the T − S spectra recorded above 50 K, also a bleaching at 545 nm was observed. The formation of the triplet giving rise to this bleaching (probably a pheophytin triplet) is related to triplet formation by the radical pair mechanism.

Keywords: D1-D2-cyt *b*-559 complex; Photosystem II; Magnetic field effects; Radical pair mechanism; Temperature dependence; Absorbance difference spectra

1. Introduction

The D1-D2-cyt *b*-559 complex, the reaction centre (RC) of Photosystem II (PS II) of plants, has been the subject of extensive spectroscopic research. The Triplet-minus-Singlet (T − S) absorbance difference spectrum of the D1-D2-cyt *b*-559 complex at low temperatures, determined with time-resolved spectroscopy [1,2], is a smooth curve without much structure. With absorbance-detected magnetic resonance (ADMR) spectroscopy it was shown that the large bleaching centred at 680 nm is generated by three types of triplets, which differ in their wavelength of maximum absorption, their $|D|$-value and their T − S spectrum [3]. The presence of triplets with different D-values was confirmed by Carbonera et al. [4], who performed fluorescence-detected magnetic resonance (FDMR). Kwa et al. [2], performing absorbance-difference spectroscopy with site-selective laser flash excitation, concluded that because of their different spectral shapes, the different triplet types indeed arise from distinct pools of P680, and cannot be explained as being analogous to the inhomogeneity observed for the P960-band of *Rhodopseudomonas viridis* [2].

In photosynthetic reaction centres in which the secondary acceptor is reduced or removed, an external magnetic field can affect the triplet yield through the so-called radical pair mechanism (RPM) [5,6] or by the magnetic

Abbreviations: ADMR, Absorbance-detected magnetic resonance; Chl, chlorophyll; ISC, intersystem crossing; LD, linear dichroic; MFE, magnetic field effect; MFI, magnetic field-induced; MIMS, magnetic field-induced mixing of triplet sublevels; MODS, magneto-optical modulation spectroscopy; Pheo, pheophytin; PS II, Photosystem II; RC, reaction centre; RP, radical pair; RPM, radical pair mechanism; T − S, triplet-minus-singlet

* Corresponding author. Fax: +31 71 275819.

SSDI 0005-2728(94)00167-7

field-induced mixing of triplet sublevels (MIMS). The latter is due to the magnetic field dependence of the eigenfunctions of the triplet state of the primary donor (^{3}P) [7]. The MIMS-effect dominates at very low temperatures (well below 60 K), and the magnetic field effect as a result of the RPM (RPM-MFE) is the principal magnetic field effect (MFE) at temperatures above 60 K.

In optical spectroscopy several applications of the MFE are known. For example, the magnetic field can be used to modulate the ground state and excited triplet state populations of one or more pigments in the sample under study. By monitoring the MFE at different wavelengths, a magnetic field-induced (MFI) T − S spectrum is obtained; this technique has been labelled magneto-optical difference spectroscopy (MODS) [7–9]. Because for recording MFI T − S spectra it is immaterial which type of MFE (MIMS or RPM-MFE) predominates, MFI T − S spectra can be recorded in a wide range of temperatures, making MODS an ideal tool for measuring temperature-dependent T − S spectra. Because the RPM-MFE is the only MFE present at higher temperatures, triplets that are formed by 'normal' intersystem crossing will not contribute to the MFI T − S spectra recorded above approx. 60 K.

The dipolar interaction, either of the triplet state of the primary radical pair (^{3}RP) or of ^{3}P, is anisotropic with respect to the direction of the external magnetic field. This offers the possibility of recording a linear-dichroic (LD) T − S spectrum, the difference of the T − S spectra obtained with light polarised parallel and perpendicular to the magnetic field. At low temperatures (where the MIMS-effect dominates) this technique allows to obtain information on, amongst others, the orientation of the optical transition moment relative to the dipole tensor of ^{3}P.

Instead of scanning the detection wavelength at a fixed magnetic field (or fixed modulation amplitude when the field is modulated), one can monitor the MFE at a fixed wavelength as a function of the magnetic field, obtaining a so-called MFE curve. The difference in MFE for light polarised parallel to the magnetic field ($MFE_{\parallel}$) and perpendicular to the magnetic field ($MFE_{\perp}$) yields the linear-dichroic (LD-)MFE curve. At high temperatures ($\geq$ 60 K), the MFE- and LD-MFE curves provide information about the interactions and kinetics involved in the formation of ^{3}P by the RPM, and on the relative orientation of the dipole tensors of ^{3}P and the radical pair triplet, respectively. At low temperatures, the curves report on the properties of ^{3}P itself. For a detailed discussion of the theoretical and technical backgrounds of the MFE, we refer to [10–12].

The D1-D2-cyt *b*-559 complex does not possess a secondary acceptor quinone, which is removed in the isolation process [13]. Consequently, the primary radical pair decays uniquely by charge recombination, and a triplet state is formed by the RPM [14] with a quantum yield > 0.8 at 10 K [14]. This makes the D1-D2-cyt *b*-559 complex a suitable candidate for a MODS study of the temperature dependence of the MFE curve and the MFI T − S spectra, analogous to the studies of Lous et al. [7,8] on bacterial RCs. These authors observed, in addition to the expected broadening of the absorption bands with increasing temperature, changes in the T − S spectra, which were ascribed to conformational changes and thermally activated energy transfer processes.

In this work, we have studied the MFI T − S spectra of the D1-D2-cyt *b*-559 complex in the range 1.2 to 200 K. It is concluded that the various bands composing the T − S spectra do not change appreciably with temperature with regard to centre wavelength, relative amplitude and width, except for the appearance of a Gaussian band centred at 674.5 nm at temperatures above 80 K. Furthermore, the temperature dependence of the MFE-curve is discussed, in relation to the temperature dependence of the MFE measured by Volk et al. [15], and the triplet yield measured by Groot et al. [16]. The LD-MFE-curve at low temperatures shows much structure, which can be explained only partly in terms of the RPM or ^{3}P parameters. Possibly, also a pheophytin triplet contributes to this structure.

2. Experimental

D1-D2-cyt *b*-559 complexes were isolated as described [13]. The sample was diluted with 66% glycerol to ascertain the formation of a clear glass. The final OD of the sample at 680 nm and room temperature was 0.4.

The MFI T − S spectra were recorded as described by Lous et al. [7], with modifications of the detection equipment as described in Ref. [17]. The data measured at 1.2 K were obtained with a home-built bath cryostat, those obtained at higher temperatures with an Oxford ESR-9 flow cryostat, equipped with a home-built pyrex insert.

The temperature was determined with a BAV 99 diode, which was placed in the sample within the light spot. The temperature was measured by monitoring the voltage across a home-built constant current supply, which provided a current of 10 μA through the diode [18,19]. The temperature dependence of the MFE was measured by simultaneously recording the voltage across the current supply of the diode and the output of a lock-in amplifier operating in 'ratio'-mode, which measured $\Delta I / I$, where I is the intensity of the transmitted light and ΔI the change in transmission induced by a (modulated) magnetic field. An AL 682 interference filter was inserted between the sample and the lamp to minimise heating effects due to the intense light.

The differential MFE was detected using field modulation. A DC magnetic field was scanned from 0 to 50 mT and a field modulation of 0.5 mT was applied with a frequency of 78 Hz. The LD-MFE was recorded either by inserting a polariser between the lamp and the sample with polarisation direction oriented parallel and perpendicular to the magnetic field, or by using isotropic excitation and inserting a photo-elastic modulator (PEM) between the sample and the detector, as in Ref. [7].

The T − S spectra recorded in the 660–695 nm region were measured with a RG 650 and a Corning filter (cut-off > 700 nm) in the excitation beam and a slitwidth of the monochromator placed between the sample and the light detector of 1 mm (0.5 nm per point). The T − S spectra ranging from 450 to 750 nm were recorded using a gray filter of 20% and a slitwidth of 2.5 mm (2 nm per point). The peak amplitude of the sinusoidally modulated magnetic field was 25 mT. (For recording T − S spectra, no DC magnetic field was applied.)

The T − S spectra were analysed using a deconvolution in Gaussian bands with software described in Ref. [3].

3. Results

The temperature dependence of the amplitude of the MFE is shown in Fig. 1. It is seen that the effect sharply decreases going from 25 to 50 K, and then, going to higher temperatures, slowly increases until a maximum is reached at 150 K, whereupon the MFE decreases. After the sample had been heated to 225 K, it was cooled and the amplitude of the MFE reached again a maximum value, which, however, was smaller than in the upgoing scan and was located at 165 K. The smaller amplitude is presumably due to degradation of the sample at temperatures above 200 K. Keeping below 200 K, we could repeatedly cycle the sample between 1.2 and 200 K with completely reversible spectral changes and amplitude of the MFE. In studying the temperature dependence of the T − S spectra, we did not record spectra above 200 K to minimise degradation of the sample.

Fig. 2a shows the MFI T − S spectra in the temperature range 1.2–200 K, recorded from 450 to 750 nm, with the amplitude of the 450–670 region amplified by a factor of 4. Fig. 2b shows the T − S spectra in the Q_y region, from 660 to 695 nm. All T − S spectra are normalised at the maximum bleaching around 680 nm. It is seen that on going to higher temperatures, the bleaching at 680 nm acquires an additional component at its blue edge, and the wavelength of maximum bleaching shifts approx. 1 nm to the red. Furthermore, the (positive) absorbance in the 450–650 nm region and at 665 nm slightly increases for temperatures above 100 K. The amplitude of the bleaching at 625 nm remains constant.

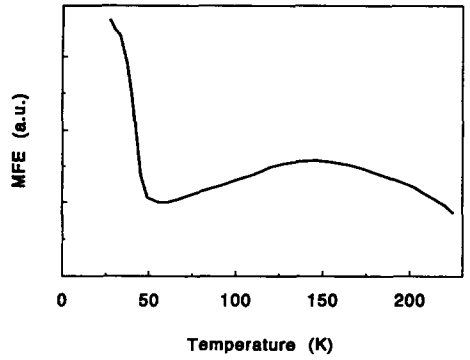

Fig. 1. Temperature dependence of the MFE of the D1-D2-cyt *b*-559 complex. The data in this figure were obained with a single temperature scan in which the temperature was slowly increased from 25 to 225 K, after which the temperature was reduced down to 120 K. The *Y*-axis shows the relative MFE ($\Delta I/I$) detected at 680 nm. The amplitude of the sinusoidal modulation was 25 mT.

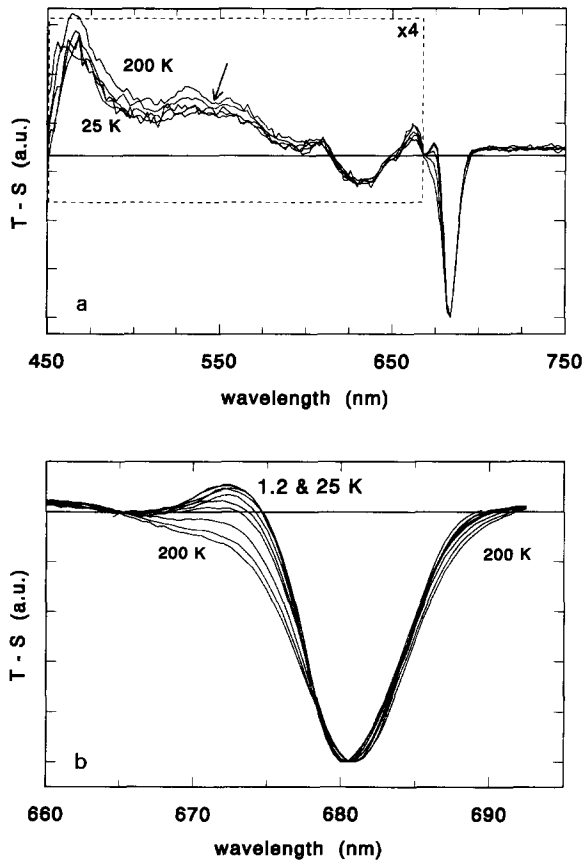

Fig. 2. Temperature dependent MFI T − S spectra of the D1-D2-cyt *b*-559 complex recorded from 1.2 to 200 K (Table 1). All spectra are normalised to the maximum absorbance difference at 680–682 nm. (a) T − S spectra in the region from 450–750 nm. The 450–670 nm region is enlarged by a factor of 4. The arrow marks the minimum at 545 nm. Spectra were recorded with a slitwidth of 2.5 mm and 2 nm per point; averages of 9 scans. (b) T − S spectra in the region from 660–695 nm. Spectra were recorded with a slitwidth of 1 mm and 0.5 nm per point; averages of 4 scans.

Fig. 3 shows the MFE recorded at 25 K (full line) and 80 K (dashed line), using field modulation, unpolarised light and a PEM with an analyser between the sample and the light detector. The (measured) derivative of the MFE-curve is displayed in the left panels (Fig. 3a and c), the (numerically integrated) actual MFE-curve in the the right panels. The upper panels show the iso-MFE-curve (Fig. 3a and b), the lower panels the LD-MFE ($MFE_{\parallel}$-$MFE_{\perp}$; Fig. 3c and d). The MFE recorded at 25 K with monochromatic light polarised parallel ($MFE_{\parallel}$; full line) and perpendicular ($MFE_{\perp}$; dashed line) to the magnetic field is shown in

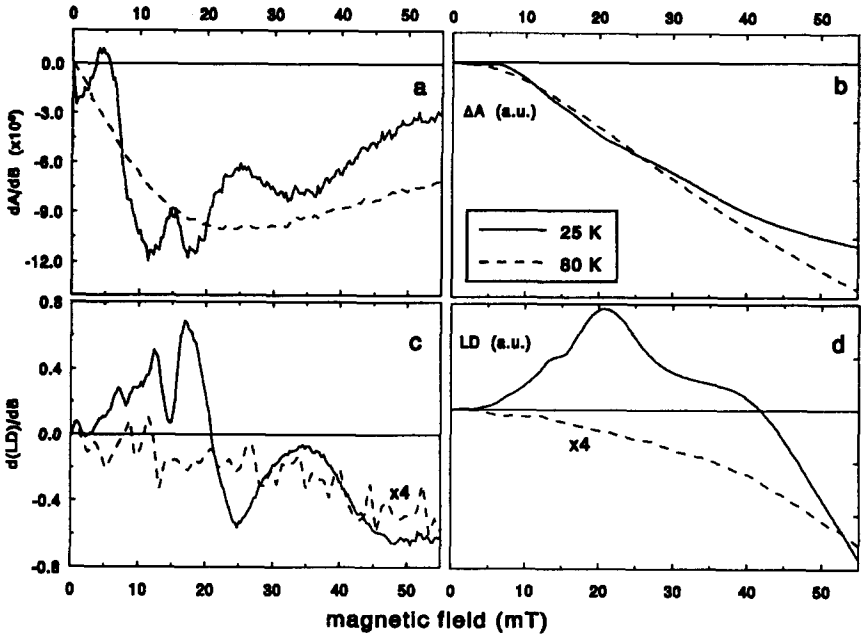

Fig. 3. Differential MFE and LD-MFE recorded at 25 K (full line) and 80 K (dashed line). The iso- and LD-MFE were recorded simultaneously using monochromatic isotropic excitation/probe light and a PEM between the sample and the detector. The field modulation had an amplitude of 0.5 mT. (a) Differential isotropic MFE; averages of 4 scans. (b) Numerically integrated MFEs from Fig. 3a. Note the possibility of the presence of a small offset in the experimental data. (c) Differential LD-MFE; averages of 4 scans. (d) Numerically integrated MFEs from Fig. 3c.

Fig. 4. The derivative MFE-curve at 25 K (resulting from a combination of MIMS and the RPM-MFE) shows much structure, which is mainly due to the $MFE_{\perp}$ (Fig. 4), as the $MFE_{\parallel}$ curve is quite smooth. In contrast, the $MFE_{\perp}$ curve shows two pronounced minima at 12 and 18 mT and a broad, weak minimum centred at 35 mT. The extremum at 4.5 mT of the iso- and LD-MFE-curves in Fig. 3a and c is also present in the $MFE_{\parallel}$ and $MFE_{\perp}$ curves (Fig. 4), although less pronounced and remaining negative. In view of the inferior signal-to-noise of the $MFE_{\perp}$ curve, recorded with half the light intensity compared to the curve of Fig. 3a, we do not attach significance to this difference. The sharp maximum at 7 mT, which is most pronounced in Fig. 3c, is reproducible, and not due to extraneous effects.

The derivative MFE recorded at 80 K is a very broad, smooth curve, with a maximum at 23 mT (the inflection point of the actual MFE). The LD-MFE is much smaller, presumably because the MFE at 80 K is completely due to the RPM-MFE, whose anisotropy is determined by the relative orientation of the dipole tensors of ^3P and ^3RP, giving rise to only a small LD-MFE. The MFE at 80 K recorded with light polarised parallel and perpendicular to the magnetic field (not shown) was identical to that measured with the PEM.

Fig. 5 shows the derivative MFE recorded with unpolarised monochromatic excitation at temperatures between 80 and 250 K (not normalised). It is seen that the maximum (corresponding to the inflection point of the MFE) moves from approx. 22 mT at 80 K to approx. 12 mT at 250 K. The maximum shifts only a few mT going from 80 to 125 K, but from 125 K to higher temperatures up to 250 K it shifts about 3 mT per 25 K. Furthermore, the amplitude of the derivative MFE at 50 mT relative to its maximum value becomes smaller with increasing temperature. This indicates that with increasing temperature the MFE saturates at lower field values.

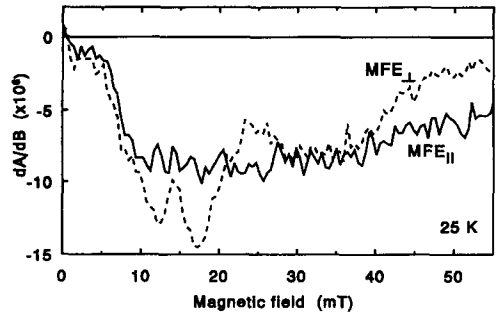

Fig. 4. Differential MFE recorded at 25 K with monochromatic excitation/probe light polarized parallel (full line) and perpendicular (dashed line) to the magnetic field; averages of 4 scans. The field modulation had an amplitude of 0.5 mT.

4. Discussion

4.1. Triplet-minus-singlet spectra between 1.2 and 200 K

The analysis of the MFI T − S spectra described below rests upon the Gaussian deconvolution of the ADMR-detected T − S spectra recorded at 1.2 K that was performed

in Ref. [3]. In this analysis, five bands were needed to fit the main bleaching of the 12 different ADMR-detected T − S spectra that were recorded at different microwave frequencies within the same resonance band. The other features of the T − S spectra were fitted with a number of additional, minor, components. Three types of triplets were discerned, corresponding to different T − S spectra: a shorter-wavelength type (characterised by two Gaussian bands with central wavelengths at 677.2 and 678.9 nm), a central-wavelength type (one Gaussian band centred at 680.4 nm, FWHM width 4.6 nm) and a longer-wavelength type (two Gaussians centred at 683.3 and 685.6 nm). In ADMR-monitored T − S spectroscopy these five bands were well discriminated because of the different zero-field splitting parameters related to these bands. In MODS, however, such a discrimination is not possible. Because the bands overlap considerably and those of a single type likely depend similarly on temperature, we have fitted the main bleaching of the MODS-recorded low-temperature

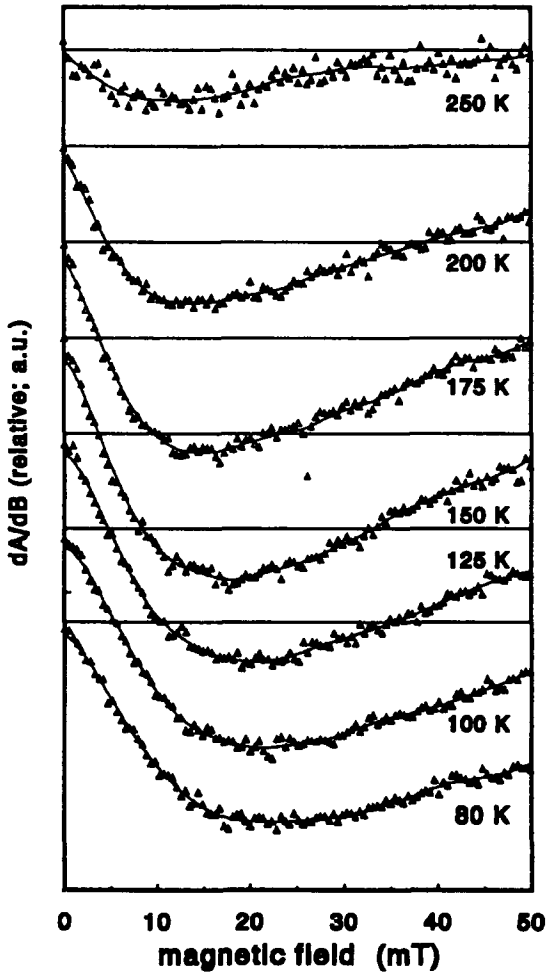

Fig. 5. Temperature-dependence of the derivative MFE recorded with monochromatic isotropic excitation light in the temperature range from 80 to 250 K. The full line is the smoothed spline function that was used to determine the maximum and $B_{1/2}$-values of the MFE-curves.

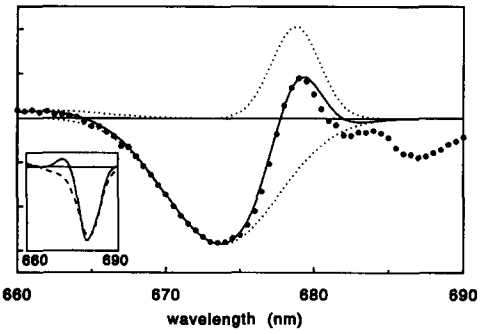

Fig. 6. Difference spectrum of the T − S spectrum recorded at 200 minus that at 25 K. Dots: difference spectrum; full line: fit; dotted lines: constituent Gaussian bands. Inset: the normalisation of the T − S spectra recorded at 25 K (full line) and 200 K (dashed line) before the difference spectrum was calculated. The normalisation was calculated as described in Ref. [3].

T − S spectra with three Gaussian bands, keeping the central band the same and substituting one band for the two shorter-wavelength bands, and one for the two longer-wavelength bands. A good fit of the T − S spectrum recorded at 1.2 K was achieved for the shorter-wavelength and longer-wavelength components having a FWHM width of 4.3 nm and 5.3 nm, respectively, and a central wavelength of 678.4 nm and 683.9 nm, respectively. For fitting the MODS-recorded 1.2 K T − S spectrum in the range 650–720 nm, three more bands were added that were previously found for the ADMR-recorded 1.2 K T − S spectrum [3]. The parameters of these three additional bands need not be varied when fitting the T − S spectra at higher temperatures. The MODS-recorded T − S spectrum at 25 K was practically identical to that recorded at 1.2 K and was fitted with the same set of bands.

Searching for possible new components that could appear at higher temperatures, we calculated the 'reduced difference spectrum' [3] of the T − S spectra recorded at 200 and 25 K (Fig. 6), and fitted this difference spectrum with three Gaussian bands. The largest band, centred at 674.5 nm with a FWHM width of 9.0 nm, corresponds to the positive feature at 672 nm of the 25 K spectrum, which has disappeared at 200 K. A second band with similar amplitude, but opposite sign, is centred at 678.4 nm and has a width of 4.5 nm, similar to that of the shorter-wavelength bleaching at 1.2 (25) K mentioned above. Apparently, the contribution of this shorter-wavelength component to the T − S spectrum is smaller at higher temperatures. A small positive component, appearing at higher temperatures, is centred at 661.9 nm, and has a width of 7.6 nm. The intensity in the difference spectrum between 680 and 690 nm is attributed to variations in width and relative amplitude of the bands that were present at low temperature. All T − S spectra recorded from 1.2 to 200 K could be described as a linear combination of the T − S spectra recorded at 25 and 200 K. Thus, with the additional components obtained from the difference spectrum

Table 1
Fit parameters of the MODS spectra of the D1-D2 complex in the Q_y-region of the spectra shown in Fig. 2

Central wavelength of the Gaussian bands (nm)	1.2 K		25 K		40 K		60 K		80 K		100 K		120 K		150 K		175 K		200 K	
661.9	−0.0058	4.7	0.0065	4.7	0.0063	4.7	0.0052	5.17	0.0090	6	0.0100	6	0.0096	6.5	0.0125	6.5	0.0142	7.63	0.0154	7.63
668.7	−0.0110	6	−0.0091	6	−0.0084	6	−0.0111	6.6	−0.0134	7.2	−0.0119	7.2	−0.0136	7.8	−0.0156	7.8	−0.0145	8.60	−0.0189	8.60
672.6	0.0250	6	0.0345	6	0.0327	6	0.0199	6.6	0.0253	6.9	0.0241	6.9	0.0185	7.8	0.0247	7.8	0.0111	9.52	0.0245	9.52
674.7	−0.0026	6	−0.0038	6	−0.0045	6	0.0092	6.6	−0.0002	7.2	−0.0091	7.2	−0.0102	7.8	−0.0384	7.8	−0.0342	9.06	−0.0540	9.06
678.4	−0.0566	4.3	−0.0573	4.3	−0.0516	4.3	−0.0545	4.73	−0.0036	5.2	−0.0068	5.2	0.0025	5.6	0.0015	5.6	0.000	7	0.000	7
680.4	−0.2257	4.6	−0.2230	4.6	−0.2090	4.6	−0.2226	5.06	−0.2647	5.8	−0.2663	6.0 [a]	−0.2619	6.5	−0.2333	6.5	−0.2294	7	−0.2044	7
683.9	−0.1706	5.3	−0.1717	5.3	−0.1612	5.3	−0.1479	5.83	−0.1378	6.0	−0.1245	6.1	−0.1133	6.9	−0.1127	6.9	−0.1086	7.12	−0.1111	7.12
710	0.0131	80	0.0051	80	0.0050	80	0.0067	80	0.0057	80	0.0072	80	0.0101	80	0.0062	80	0.0031	80	−0.0003	80

At each temperature, the amplitude of the Gaussian bands, normalised on the sum of the oscillator strengths (computed as amplitude × sqrt(width)) of the four major bleaching bands centered at 674.7, 678.4, 680.4 and 683.9 nm (left column) and FWHM of the bands in nm (right column) are given.

[a] Center: 680.5 nm.

of Fig. 6, we have the full set of Gaussian bands that fits the MFI T − S spectra over the entire temperature range. Fig. 7 shows the fits for the T − S spectra recorded at 25, 80, 120 and 200 K; all other T − S spectra could be fitted equally well. Table 1 lists the parameters used in the fits of the T − S spectra; Fig. 8 shows the oscillator strength of the major Gaussian bands as a function of the temperature. The oscillator strengths of Fig. 8 and Table 1 have been normalised to the total optical strength of the major bleaching bands. Going from 1.2 to 200 K, the bands broaden with a factor varying from 1.4 to 1.6. The shift of the band centred at 683.9 nm is negligible (+0.1 nm). The contribution of the 678.4 nm band (the shorter-wavelength triplet type) to the low-temperature MFI T − S spectrum is much smaller than in the analysis of Ref. [3]. Because the mechanism that gives rise to the modulation in triplet concentration is different for ADMR and MODS, the presence of the same triplet states might give rise to a different ΔA when measured with the two techniques, thus changing the composition of the T − S spectrum. On the other hand, in Ref. [3] it was shown that especially the 678.4 nm component is sensitive to the isolation procedure, and we cannot exclude that, in spite of the same overall isolation procedure, the samples of Ref. [3] were slightly different from the present ones.

From Fig. 8 it is seen that the shorter-wavelength component (678.4 nm) of the main bleaching vanishes at temperatures above 60 K, with a concomitant increase in amplitude of the 680.4 nm component. This suggests that between 60 and 80 K the shorter-wavelength triplet transforms into the central-wavelength triplet. The short-wavelength, low-temperature triplet could be due to a Chl present in the D1-D2-cyt *b*-559 complex other than P, or, as proposed in Ref. [3], due to P in RCs with a different

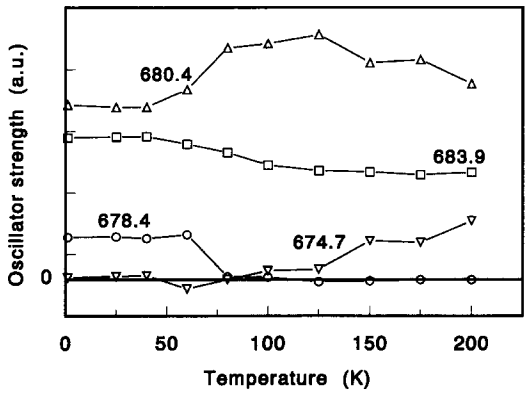

Fig. 8. Oscillator strengths of the components contributing to the main bleaching in the MFI T − S spectra from 1.2 to 200 K. The total oscillator strength present in the main bleaching is normalised at each temperature. For more information about the parameters used, see text and Table 1.

conformation. A similar change can be observed in the CD spectra recorded at different temperatures. The CD spectrum of the D1-D2 complex at 6 K measured by Otte et al. [20], shows a positive contribution at 675 nm, which is absent in CD spectra measured at 77 K [21,22]. Studying the temperature dependence of the CD spectrum from 6 to 298 K every 50 K, it was found (C. Francke, unpublished results) that the feature at 675 nm is still present in the CD spectrum recorded at 50 K, but is absent in the CD spectrum recorded at 100 K. We conclude that the differences between the 6 K CD spectrum [20] and the 77 K CD spectrum [21,22] are not caused by differences in the preparation used, but are a property of the D1-D2 complex itself, resulting, for example, from a conformational change. This suggests that the change observed in the MFI T − S spectra between 50 and 70 K is not due to a

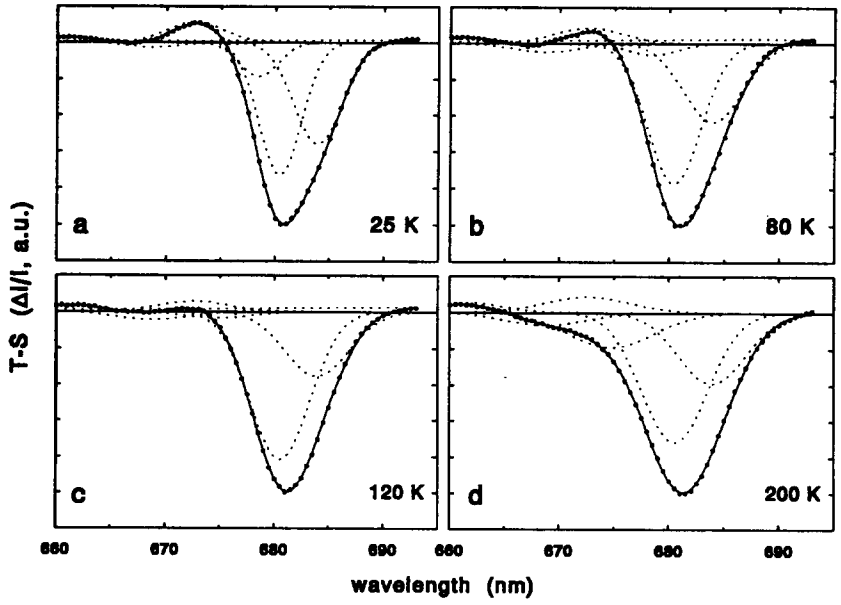

Fig. 7. Fits of the MFI T − S spectra recorded at (a) 25 K, (b) 80 K, (c) 120 K and (d) 200 K. The spectra at 1.2, 25 and 40 K are practically identical with similar fit parameters (Table 1).

de-trapping of the shorter-wavelength triplet state, but is caused by a change in interaction of this triplet state with its environment.

A Gaussian band centred at 674.7 nm appears at temperatures above 80 K and acquires a significant amplitude above 120 K (Fig. 8). Taking a closer look at the components of the main bleaching, the contribution of the 680.4 nm band is seen to begin to decrease close to the temperature at which the 674.7 nm band comes up. The numerical correlation between the 674.7 and 680.4 nm bands implies a physical relationship and suggests that the triplet state of one of the (primary donor) Chls present at low temperatures delocalises to an adjoining pigment. Such a delocalisation is also observed for the primary donor triplet of PS I, which at low temperature is localised on one of the two Chls of the dimeric primary donor, and at higher temperatures delocalises over these two Chls [23].

The 500–600 nm region of the MFI T − S spectra shows a minimum at 545 nm. This minimum is present in all T − S spectra recorded at temperatures above 50 K. The S/N ratio in the T − S spectra at low temperatures around 545 nm is too low to draw conclusions about a possible correlation between the minimum at 545 nm and the appearing band at 674.7 nm in the Q_y region. In the ADMR-detected T − S spectrum of P680 there is no minimum between 540 and 560 nm. Instead, a broad, positive band, which is maximal at about 550 nm, is observed [24]. Pheophytin, however, shows a T − S spectrum with a sharp, deep minimum at 546.5 nm [25]. Assuming that the 545 nm minimum of the high-temperature MFI T − S spectra is due to ^{3}Pheo, and using the ^{3}Pheo T − S spectrum of Ref. [25] as calibration, we calculate that at 200 K ^{3}Pheo contributes 15% of the T − S spectrum, the remaining major part being due to Chl triplets.

It was argued that the ^{3}Pheo triplet was formed via the RPM followed by triplet energy transfer [3] [1], but recent experiments of Carbonera et al. [4] show that the pheophytin triplet yield does not change after treatment with Triton X-100, which reversibly deactivates the RC [26]. It follows that the pheophytin triplet detected with ADMR at low temperatures is not formed by the RPM, and that it is not due to a Triton X-100-induced contamination or change in RC structure. Presumably, at low temperature the pheophytin absorbing at 680 nm acts as a trap for triplets formed by intersystem crossing. Whether the triplet attributed to pheophytin in the present high-temperature experiments is located on the 680 nm pheophytin or on the (active) pheophytin absorbing at 676 nm [1] cannot be decided here. The fact that it is magnetic-field sensitive above 50 K shows that it is not formed by intersystem crossing, but is related to triplet formation via the RPM. This suggests that at higher temperatures there is either some triplet transfer from ^{3}P680 to the observed pheophytin, or partial recombination of the radical pair to the pheophytin triplet state.

4.2. Magnetic field effect below 60 K

The derivative (LD-)MFE-curve recorded at 25 K, monitoring at 680 nm, is characterised by several local maxima and minima, which cannot be understood easily in terms of the parameters of ^{3}P and ^{3}RP. The low-temperature (LD-)MFE-curve of the D1-D2-cyt *b*-559 complex has a much sharper structure than that of RCs of purple bacteria [12]. For example, the (LD-)MFE-curve of RCs of *Rb. sphaeroides* shows two broad, just-resolved maxima at 12 and 21 mT, compared to the sharply defined maxima at 12.5 and 17 mT for the D1-D2-cyt *b*-559 complex. Comparison of the (LD-)MFE-curves of quinone-depleted RCs and RCs containing a pre-reduced quinone indicated that the double maximum for bacterial RCs is probably due to the presence of a negatively charged quinone, so that its presence in the quinone-less D1-D2-cyt *b*-559 complex is quite surprising. A further important difference between the bacterial and PS II (LD-)MFE-curves is the region below 10 mT. For RCs from purple bacteria, the derivative of the MFE-curve shows a sharp negative peak, which crosses the baseline at approx. 9.8 mT. For the D1-D2-cyt *b*-559 complex, however, this negative peak is completely absent; at 7 mT only a small, positive local maximum is observed. In contrast to bacterial RCs, the $MFE_{\perp}$ curve of the RCs of PS II increases faster at low magnetic field strengths than the $MFE_{||}$ curve, so that the LD-MFE remains positive at field strengths below 10 mT.

Angerhofer et al. [27], who performed a magnetic field-dependent ADMR study, suggested that the positive part of the low-temperature derivative MFE, reaching a maximum at 4.7 mT (an increase of the MFE), is due to a so-called $2J$-resonance. The purported $2J$-resonance should also be present in the high-temperature MFE-curve, as a $2J$-resonance is a characteristic of the RPM-MFE. MFE-curves recorded above 60 K, however, do not show a $2J$-resonance at all (Fig. 5). We therefore conclude that the peak at 4.5 mT observed at low temperatures is not a $2J$-resonance, but is generated by the MIMS effect.

4.3. Magnetic field effect above 60 K

The temperature-dependence of the MFE recorded using sinusoidal modulation with an amplitude of 25 mT (Fig. 1) shows three conspicuous features: A sharp decrease in amplitude when going from 25 to 50 K, a slow increase going from 50 to 175 K, and a decrease when going upwards from 175 K. The first feature can be

[1] Assignment of ^{3}Pheo formation to the RPM was largely based on a microwave double-resonance experiment; later experimentation has shown that the observed effect may have been due to microwave interference (Angerhofer, A., private communication and van der Vos, R., unpublished experiments).

explained by considering the different mechanisms that play a role in the MFE: the MIMS-effect and the RPM-MFE. The MIMS-effect is only effective at low temperatures when the triplet sublevels are not connected by spin-lattice relaxation. Thus, the decrease in amplitude of the MFE is probably due to the decreasing amplitude of the MIMS-effect. The temperature at which the MIMS-effect seems to have disappeared (approx. 60 K) agrees with the temperature at which the low-temperature MFE-curve (Fig. 3, 25 K) transforms into the high-temperature MFE-curve (Fig. 3, 80 K). A similar temperature dependence of the MFE was observed for bacterial RCs [8,9].

The temperature dependence of the MFE above 50 K should be described in terms of the kinetic parameters that are involved in the RPM and in other primary electron transport processes. An increase in amplitude of the RPM-MFE can be due to an increase of the triplet yield or of the efficiency of the MFE. Which parameters are likely to change cannot be inferred from the data of Fig. 1 alone. The analysis of the temperature dependence of the MFE (Fig. 5) and of time-resolved spectroscopy at different temperatures should be included in a quantitative discussion of the temperature dependence of the triplet yield and the efficiency of the MFE.

Groot et al. [16] calculated the triplet and fluorescence yield as a function of temperature using a complicated four-compartment model in which excitation energy was transferred between the primary donor and different chlorophylls of the D1-D2 complex, the rates which were all thermally activated. In addition, the fluorescence was assumed to compete with internal conversion, the latter being also thermally activated, so that the fluorescence yield became less at higher temperatures. Groot et al. neglected triplet formation by intersystem crossing, and used temperature-independent rates for the formation of triplets by the radical pair mechanism and for charge recombination to the singlet ground state. The free energy of charge separation resulting from the model was in fact a distribution of activation energies represented by values of 20, 40 and 80 meV. The detailed model of Groot et al. provides a reasonable fit of the triplet and fluorescence yield data, but fails to account for the data on the magnetic field effect on the triplet yield. We therefore develop a rather different model for the observed temperature dependence of the MFE and of the triplet yield, which, although fairly simple, properly takes into account the spin dynamics of the primary donor pair. Our model fits all available triplet yield data including those of Ref. [16] reasonably well, and could serve as a starting point for a more detailed description, including for example the temperature dependence of the fluorescence and its magnetic field effect.

Consider the energy level scheme drawn in Fig. 9. The excited primary donor state P^*I decays with rate $k_{Fl} + k_{IC}$ to its ground state, PI. For this rate, we take the in vitro fluorescence rate of Chl *a*, 0.06 ns^{-1} [28]. (The measured recombination fluorescence rates of 0.05 and 0.014 ns^{-1}

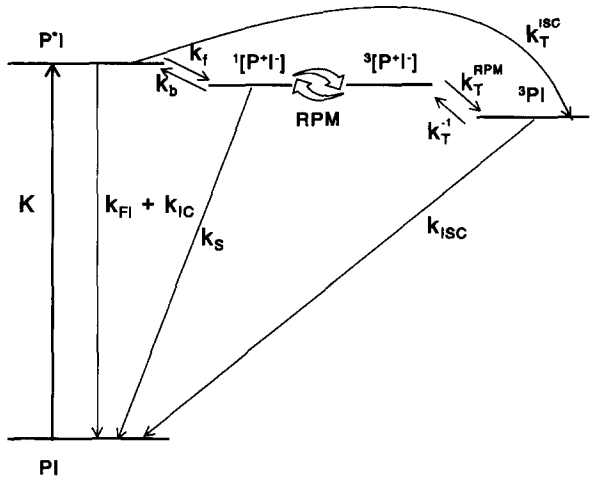

Fig. 9. Energy scheme for radical pair and triplet formation and decay for the D1-D2-cyt *b*-559 complex of PS II.

[29], are a combination of the actual fluorescence rate, the equilibrium between P^* and ^1RP, and the decay rates of ^1RP, and therefore do not represent the actual value of k_{Fl}.) The radical pair singlet state (^1RP) formed by charge separation with rate $k_f \approx 300$ ns^{-1} [30] recombines to the ground state PI with rate k_S, determined by Volk et al. to be 0.002 ns^{-1} at 90 K and 0.01 ns^{-1} at 290 K [15], or to the singlet excited state of the primary donor, P^*, with rate k_b. This rate was modelled by a thermally-activated charge recombination from ^1RP to P^*I, with rate $k_b = k_f \exp(-\Delta G_{cs}/k_BT)$, where ΔG_{cs} is the free energy difference between the P^*I and $^1[P^+I^-]$ state, k_f the rate of charge separation from P^*, k_B Boltzmann's constant and T the temperature. We include in our model formation of the primary donor triplet state ^3P by the radical pair mechanism with recombination rate (k_T^{RPM} approx. 5 ns^{-1} [15]) and by intersystem crossing (ISC) with rate k_T^{ISC}. From in vitro measurements it was concluded that the quantum yields for fluorescence and triplet state formation are 32% and 64%, respectively (direct internal conversion has a low probability), implying that the rate of triplet formation is twice that for fluorescence [32], which yields $k_T^{ISC} = 0.11$ ns^{-1}. For the primary donor of the D1-D2 complex, the rate of internal conversion (k_{IC}) could be much larger than for Chl *a* in vitro [16], therefore in our simulation k_{IC} was used as a free parameter. The primary donor triplet state decays to the ground state by ISC, with rate $k_{ISC} = 0.6$ ms^{-1} [24], and by thermally-activated triplet charge separation with rate k_T^{-1} [15,33]. The set of differential equations for the model represented by Fig. 9 is

$$\frac{d[P]}{dt} = -K[P] + (k_{Fl} + k_{IC})[P^*] + k_S[^1RP] + k_{ISC}[^3P] \quad (1)$$

$$\frac{d[P^*]}{dt} = -\left(k_{Fl} + k_{IC} + k_f + k_T^{ISC}\right)[P^*] + k_b[^1RP] \quad (2)$$

$$\frac{d[^3P]}{dt} = -(k_{ISC} + k_T^{-1})[^3P] + k_T^{RPM}[^3RP] + k_T^{ISC}[P^*] \quad (3)$$

$$\frac{d[\rho]}{dt} = -\frac{i}{\hbar}[H,\rho] - \tfrac{1}{2}(k_S + k_b)[P_S,\rho]_+ - \tfrac{1}{2}k_T^{RPM}[P_T,\rho]_+ + k_f[P^*](P_S I P_S) + k_T^{-1}[^3P](P_T I P_T) \quad (4)$$

with

$$[^1RP] = Tr(P_S\rho) \text{ and } [^3RP] = Tr(P_T\rho) \quad (5a,b)$$

and the boundary condition

$$[P] + [P^*] + [^1RP] + [^3RP] + [^3P] = 1 \quad (6)$$

where K is the excitation flux (set to 950 s^{-1}); all other rates and components were defined above. $[X]$ represents the concentration of component X, $[X,Y]$ the commutator $XY - YX$, and $[X,Y]_+$ the anti-commutator $XY + YX$. H is the Hamiltonian, ρ the density matrix of the radical pair, and I the identity matrix. The diagonal elements of ρ represent the probability that the radical pair recombines to a specific electron spin state, which can be selected by the singlet and triplet projection operators, P_S and P_T, respectively. The trace of $P_S\rho$ and $P_T\rho$, the probability that the radical pair is in the singlet or in the triplet state [6,11], is represented by the pseudo-concentrations $[^1RP]$ and $[^3RP]$, respectively. The non-diagonal elements of ρ represent the transition probabilities between the electron spin states of the radical pair, and are determined by the energy differences of the radical pair singlet and triplet levels, the hyperfine interactions and the difference in g-value of the two radical pair components. For bacterial RCs, the term of Eq. (4) containing k_f is usually ignored, because the charge-separation rate k_f is much faster than the dynamics of the radical pair and the rate of recombination to P^*. The time evolution of the density matrix is then calculated with the starting condition that all molecules are in the charge-separated singlet state. In our case, however, the back reaction rate k_b is thought to play an important role, as it could have an appreciable effect on the triplet yield [31]. For $k_b \geq k_S$, and $k_f \gg k_{Fl}$, a considerable part of the loss of radical pair singlet states given by $(k_S + k_b)[^1RP]$ is not 'lost', but recombines to the primary donor excited state P^*, after which almost immediately again a radical pair is formed (in the singlet state). Thus, the effect of a fast charge recombination rate k_b on the triplet yield is *not* that the ^1RP state decays by $(k_b + k_S)$ in stead of k_S, leaving a smaller radical pair population to recombine to ^3P by the RPM, but that an equilibrium is established between the ^1RP and P^* states. Note that, when k_b increases, the average time at which the spin evolution of the radical pair is interrupted, is reduced. This diminishes the average triplet character of the radical pair, resulting in a lower triplet yield [6].

Haberkorn et al. [34] derived an expression for an effective decay rate for the case of two radical pairs between which electron hopping occurred, one of the radical pairs recombining to the ground state with recombination rate k_S. There are two important differences between the hopping model of Haberkorn et al. and our system: First of all, our two states between which hopping occurs *both* have a direct decay channel to the ground state. This makes it impossible to derive expressions for the fluorescence yield and the amount of recombination from the radical pair to the ground state, without making further assumptions about the relative concentrations of P^* and ^1RP. Secondly, in our case the hopping process occurs between the singlet part of the radical pair and the P^* state, in contrast to the system of Haberkorn et al. [34] where the hopping occurred between two radical pairs, with conservation of singlet/triplet character. Therefore, the system of Haberkorn et al. and ours are not isomorphous as was stated in Ref. [35], and we cannot substitute the $^1P^*$ – state and the ^1RP state for the 'Distant' and 'Close' radical pair, respectively, of Haberkorn et al. [34], as in [35].

The effect of a magnetic field when electron hopping is included in the Liouville equation was calculated in [5]. We take a somewhat different approach, which yields the triplet yield under steady-state conditions. First, we calculate the triplet yield for a radical pair that is populated only once in the singlet state and whose singlet and triplet states recombine with rates $(k_b + k_S)$, and k_T^{RPM}, respectively, with the equations from Haberkorn et al. for the one-proton model [6]. We neglect the source term with k_T^{-1} in Eq. (4), because at all temperatures, $k_T^{-1} \ll k_T^{RPM}$. The triplet yield of a radical pair created in the singlet state at zero field is [6]

$$\Phi_T(0) = 3(A/\hbar)^2 k_T^{RPM}\left((k_S + k_b) + k_T^{RPM}\right) / \left\{\left[3(A/\hbar)^2 + 4(k_S + k_b)k_T^{RPM}\right] \times \left((k_S + k_b) + k_T^{RPM}\right)^2 + 16(k_S + k_b)k_T^{RPM}(J - A/2)^2/\hbar^2\right\}, \quad (7)$$

and at infinite magnetic field

$$\Phi_T(\infty) = (A/\hbar)^2 k_T^{RPM}\left((k_S + k_b) + k_T^{RPM}\right) / \left\{\left[(A/\hbar)^2 + 4(k_S + k_b)k_T^{RPM}\right] \times \left((k_S + k_b) + k_T^{RPM}\right)^2 + 16(k_S + k_b)k_T^{RPM}(J/\hbar)^2\right\}. \quad (8)$$

In Eqs. (7) and (8), the driving force of singlet–triplet mixing is the hyperfine interaction; the difference in g-value of the two radicals is neglected. From the EPR-linewidth, the average hyperfine interaction of P^+ is estimated to be 8 G [36], and that of I^- 13 G [37], resulting in an

effective one-proton hyperfine interaction A of 15.26 G [6]. If there is no charge recombination to P^*, i.e. $k_b = 0$, then, for $k_f \gg k_{Fl}$, the triplet yield calculated with Eq. (7) should equal the actual triplet yield of the system.

We will now introduce a kinetic model, from which the steady-state concentrations of the states of Fig. 9 will be calculated. The model is based on the idea that if a steady-state situation is obtained, there exists an effective mixing rate k_{ST}, which can be substituted for the radical pair mechanism. In this kinetic model, Eq. (4) is split into

$$\frac{d[^1RP]}{dt} = k_f[P^*] - (k_b + k_S + k_{ST})[^1RP] \quad (4a)$$

and

$$\frac{d[^3RP]}{dt} = k_{ST}[^1RP] - k_T^{RPM}[^3RP]. \quad (4b)$$

The effective mixing rate k_{ST} is defined by

$$\Phi_T(B) = \frac{k_{ST}(B)}{k_S + k_b + k_{ST}(B)}$$

resulting in

$$k_{ST}(B) = \frac{\Phi_T(B)(k_S + k_b)}{(1 - \Phi_T(B))}, \quad (9)$$

so that every time a radical pair is formed, the triplet yield equals that calculated with Eqs. (7) or (8). The steady-state concentrations are calculated by calculating $k_{ST}(B)$ for $B = 0$ and ∞, setting the time-derivatives of Eqs. (1)–(4b) to zero, and solving the resulting system of linear equations, using Eq. (6) as a boundary condition. The difference in ^3P concentration for $B = 0$ and ∞ multiplied by $(k_{ISC} + k_T^{-1})$ gives the MFE on the yield of ^3P.

In a first simulation, we kept k_S constant; as all rate constants involved in the model are relatively well known, the only free parameters of the simulation are the free energy difference ΔG_{cs}, which was expected to determine the characteristics of the broad maximum in Fig. 1, and the rate of internal conversion, k_{IC}. The latter proved to be an important parameter in determining the triplet yield at temperatures above 200 K. If the triplet formation by ISC was neglected, the free energy difference ΔG_{cs} indeed determined the temperature at which the MFE started to increase and where it was maximal. Quite surprisingly, however, if k_T^{ISC} was included in the simulation, then ΔG_{cs} determined the temperature at which the MFE started to *decrease*, and no maximum was observed. Apparently, the small value of k_T^{ISC} ($< 0.1\%$ of k_f) becomes important, if the P^* level is repeatedly populated by the hopping between ^1RP and P^*. In that case, primary donor triplets are also formed by ISC. In a next step, we introduced a thermally-activated ^1RP decay rate $k_S(T)$, of the form:

$$k_S(T) = k_S^o + K_S e^{(\frac{\Delta E_{ks}}{k_B T})}, \quad (10)$$

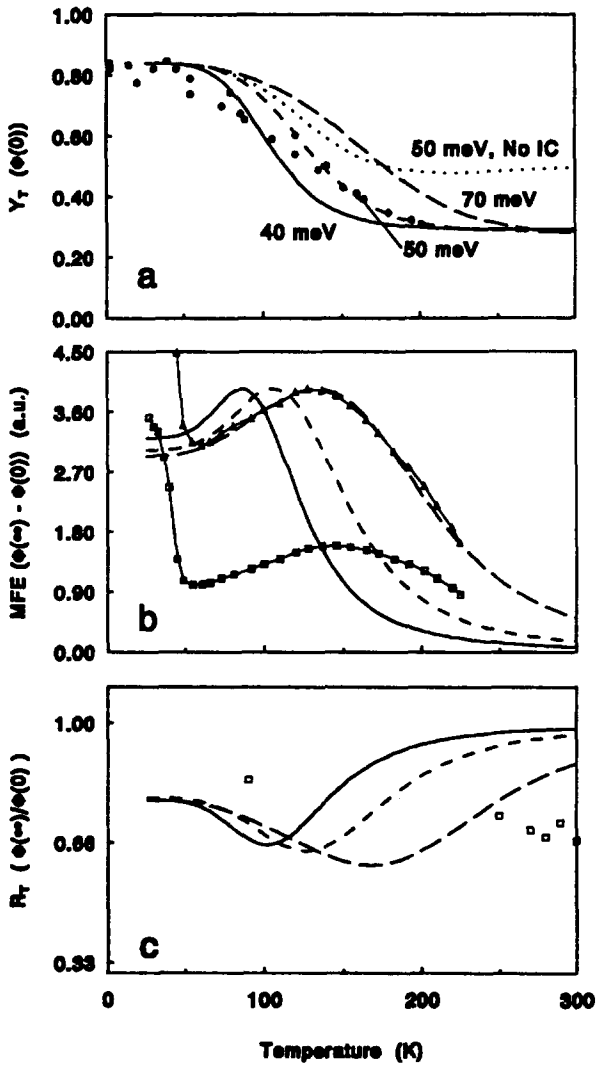

Fig. 10. Simulations of the temperature dependence of the triplet yield without magnetic field ($\Phi(0)$) and with a saturating magnetic field ($\Phi(\infty)$) for different experimental data. The simulations were performed for a free energy of charge separation (ΔG_{cs} of -40 meV (full line), -50 meV (short-dashed line) and -70 meV (long-dashed line)). (a) The triplet yield ($\Phi(0)$) measured by Groot et al. [16] (●). Dotted line: simulation of the triplet yield with $\Delta G_{cs} = -50$ meV and no internal conversion ($k_{IC} = 0$). (b) The MFE measured in this work (□), and corrected for the effect of the non-saturating magnetic field (▲), as described in the text. The simulated curves represent $\Phi(0) - \Phi(\infty)$ for values of ΔG_{cs} as in Fig. 10a; they are normalised on their (local) maximum. (c) The MFE ratio, $\Phi(\infty)/\Phi(0)$, measured by Volk et al. [15] (□). Simulated curves calculated for values of ΔG_{cs} as in Fig. 10a.

where k_S^o represents the constant low-temperature rate of recombination when nuclear tunnelling takes over. Fig. 10 shows the simulation with $k_S^o = 0.0020$ ns^{-1}, $K_S = 0.022$ ns^{-1}, $\Delta E_{ks} = -26$ meV, and $\Delta G_{cs} = -40$, -50 or -70 meV.

Fig. 10a shows the data of the triplet yield measured by Groot et al. [16] and our simulation. It is seen that the data are simulated best when ΔG_{cs} is between -40 and -50 meV. For illustration, the triplet yield is simulated also for

the case that there is no internal conversion. Introducing a thermally-activated internal conversion and a distribution of energies as in Groot et al., could further improve the simulation, but that is beyond the scope of this work. k_S^o was chosen such that the triplet yield at low temperatures equalled that measured by Groot et al. [16]. In our model, recombination of the singlet radical pair to P^* provides a loss channel in the radical pair mechanism, lowering the RPM triplet yield appreciably at higher temperatures. At $T > 200$ K, the calculated yield is almost constant, in good agreement with the measured yield ([14,16,38]; E. Franken, unpublished results).

The dependence on the temperature of the magnetic field effect presented in this work, could not be simulated as straightforward as that of the triplet yield. Eq. (8) holds for the triplet yield at infinite magnetic field. However, the maximal magnetic field of our Helmholtz coils was not infinite, but approx. 25 mT. Volk et al. determined that the magnetic field at which the MFE reached half of its value in saturation ($B_{1/2}$) changed from 340 G at 90 K to 190 G at 290 K. This dependence of $B_{1/2}$ on T implies that the MFE measured by us is not a constant fraction of the (theoretical) maximal difference, but that this fraction changes with temperature. Assuming a Lorentzian shape of the magnetic field dependence of the triplet yield, the MFE measured can be represented by (M. Volk, personal communication)

$$MFE = (\Phi(0) - \Phi(\infty))\left(\frac{B^2}{B^2 + B_{1/2}^2}\right) \qquad (12)$$

We approximated the temperature dependence of $B_{1/2}$ by interpolating $B_{1/2}$ linearly between the two values of $B_{1/2}$ measured by Volk et al. at 90 and 290 K [15]. Dividing the measured data by the factor resulting from the Lorentzian shape, results in an MFE-curve that can be compared with the theoretically calculated curves. Fig. 10b shows the 'corrected' data together with the simulated MFE-curves. It is seen that the curve for $\Delta G_{cs} = -70$ meV fits the data quite well, whereas the maxima for $\Delta G_{cs} = -40$ and -50 meV are located at temperatures that are lower than that of the experimentally determined maximum. Although a free energy difference of -70 meV is somewhat higher than that found in the simulation of the temperature dependence of the triplet yield (see above), we feel that considering the rather crude approximation made for the temperature dependence of $B_{1/2}$, the agreement between the two independent simulations is satisfactory.

Above, we have simulated the temperature dependence of the triplet yield ($\Phi(0)$) and the magnetic field effect ($\Phi(\infty) - \Phi(0)$). As a further test of our model, we also simulated the temperature dependence of the relative magnetic field effect, that is $\Phi(\infty)/\Phi(0)$, which was measured by Volk et al. [15]. The simulation and the data of Volk et al. are shown in Fig. 10c. The simulated ratio is approx. 0.65 at 20 K, steadily decreases with increasing temperature, reaches a minimum between 100 and 200 K, and increases with further warming (Fig. 10c). In the high temperature limit, well above 300 K, the ratio equals unity. The initial decrease of the ratio, at temperatures between 75 K to 190 K, is due to the decrease in triplet yield, from a value close to unity, where the MFE is small (for 100% triplet yield there is only one decay channel of the radical pair, and the presence of a magnetic field does not affect the yield), to about 0.3, where the MFE approaches its maximum value. On further warming, k_b increases and due to the repopulation of P^*, a considerable amount of triplets is then formed by ISC. Because the yield of the triplets formed by ISC contributes to the overall triplet yield, but does not depend on the magnetic field, the ratio $\Phi(\infty)/\Phi(0)$ increases [2]. Our simulations show that for a broad range of ΔG_{cs} values, the triplet yield at room temperature contains a large contribution of triplets formed by ISC. Note, however, that at 300 K our simulated values of $\Phi(B = \infty)/\Phi(B = 0)$ are always considerably higher than the ratios measured by Volk et al. It proved not possible to achieve a better fit without compromising the fits of Fig. 10a,b. This might be due to the relative simplicity of our model. For example, taking nuclear spin polarisation into account would depress the relative yield of triplets formed by the RPM [39]. At higher temperatures increased spin-lattice relaxation lowers the extent of nuclear polarisation, thus lowering the calculated ratio $\Phi(\infty)/\Phi(0)$. Before extending our model, however, further experimentation is needed, for example for verifying the occurrence of a minimum in the temperature dependence of $\Phi(\infty)/\Phi(0)$ as predicted by our simulations.

5. Conclusions

The (LD-)MFE-curve of the D1-D2 complex recorded at 25 K, shows more structure than that recorded for RCs of *Rb. sphaeroides* wild-type. The additional structure cannot be due solely to the differences in the zero-field parameters of ^3P; possibly, it is due to a pheophytin triplet, or to as yet unknown environmental factors.

The temperature dependence of the magnetic field-induced T − S spectra was small. The shorter-wavelength triplet type disappears between 50 and 70 K, and is probably converted into the central-wavelength triplet type. At temperatures above 120 K, the T − S spectrum shows a new bleaching, centred at 674.5 nm.

[2] For example, if half of the triplet yield is formed by ISC (Y_{ISC}), and half of the triplets by the RPM (Y_{RPM}), and the MFE reduces Y_{RPM} by one third, the ratio $\Phi(\infty)/\Phi(0)$ becomes

$$\frac{\Phi(\infty)}{\Phi(0)} = \frac{Y_{ISC} + \frac{1}{3}Y_{RPM}}{Y_{ISC} + Y_{RPM}} = \frac{2}{3},$$

much larger than expected for the actual MFE.

The temperature dependence of the amplitude of the MFE between 50 and 200 K is discussed in the framework of a kinetic model, in which the steady-state population of the different primary donor states are calculated, using expressions for the triplet yields derived by Haberkorn et al. [6]. The maximum of the MFE observed at approx. 150 K is ascribed to a thermally-activated rate of charge recombination from the radical pair singlet state to the singlet ground state, k_S. At higher temperatures, triplet formation by ISC becomes important because of thermally-activated charge recombination from ^{1}RP to P*. We predict a minimum in the MFE ratio $\Phi(\infty)/\Phi(0)$ between 100 and 200 K.

Acknowledgements

We thank Dr. Peter van Leeuwen and Benny van Buel for expertly isolating the D1-D2 complexes, Christof Francke for measuring the CD-spectra, M. Groot for making Ref. 16 available prior to publication and Drs. P.J. Hore, A. Ogrodnik and M. Volk for fruitful discussions. This work was supported by the Netherlands Foundation for Chemical Research (SON), financed by the Netherlands Organisation for Scientific Research (NWO).

References

[1] Van Kan, P.J.M., Otte, S.C.M., Kleinherenbrink, F.A.M., Nieveen, M.C., Aartsma, T.J. and Van Gorkom, H.J. (1990) Biochim. Biophys. Acta 1020, 146–152.
[2] Kwa, S.L.S, Eijckelhoff, C., Van Grondelle, R. and Dekker, J.P. (1994) J. Phys. Chem. 98, 7702–7711.
[3] Van der Vos, R., Van Leeuwen, P.J., Braun, P. and Hoff, A.J. (1992) Biochim. Biophys. Acta 1140, 184–198.
[4] Carbonera, D., Di Valentin, M. and Giacometti, G. (1994) Biochim. Biophys. Acta 1185, 167–176.
[5] Werner, H.-J., Schulten, K. and Weller, A. (1978) Biochim. Biophys. Acta 502, 255–268.
[6] Haberkorn, R. and Michel-Beyerle, M.E. (1979) Biophys. J. 26, 489–498.
[7] Lous, E.J. and Hoff, A.J. (1988) in The Photosynthetic Bacterial Reaction Center -Structure and Dynamics (Breton, J. and Verméglio, A., eds.), pp. 71–88, Plenum, New York.
[8] Lous, E.J. and Hoff, A.J. (1986) Photosynth. Res. 9, 89–101.
[9] Lous, E.J. and Hoff, A.J. (1989) Biochim. Biophys. Acta 974, 88–103.
[10] Hoff, A.J., Gast, P., Van der Vos, R., Vrieze, J., Franken, E.M. and Lous, E.J. (1993) Z. f. Phys. Chem., Bd. 180, 175–192.
[11] Hoff, A.J. (1981) Q. Rev. Biophys. 14, 599–665.
[12] Van der Vos, R., Franken, E.M., Sexton, S.J., Shochat, S., Gast, P., Hore, P.J. and Hoff, A.J. (1994) Biochim. Biophys. Acta, in press.
[13] Van Leeuwen, P.J., Nieveen, M.C., Van de Meent, E.J., Dekker, J.P. and Van Gorkom, H.J. (1991) Photosynth. Res. 28, 149–153.
[14] Takahashi, Y., Hansson, Ö., Mathis, P. and Satoh, K. (1987) Biochim. Biophys. Acta 893, 49–59.
[15] Volk, M., Gilbert, M., Rousseau, G., Richter, M., Ogrodnik, A. and Michel-Beyerle, M.-E. (1993) FEBS Lett. 336, 357–362.
[16] Groot, M.L., Peterman, E.J.G., Van Stokkum, I.H.M., Van Kan, P.J.M., Dekker, P.J. and Van Grondelle, R. (1994) Biophys. J. 67, 318–330.
[17] Van der Vos, R. Carbonera, D. and Hoff, A.J. (1991) J. Appl. Magn. Res. 2, 179–202.
[18] Van Kan, P.J.M. (1991) Doctoral Dissertation, Leiden.
[19] Rao, M.G. (1982) in Temperature, its Measurement and Control in Science and Industry, Vol. 5, pp. 1205–1211, American Institute of Physics, New York.
[20] Otte, S.C.M., Van der Vos, R. and Van Gorkom, H.J. (1992) J. Photochem. Photobiol. (B) 15, 5–14.
[21] Tetenkin, V.L., Gulyaev, B.A., Seibert, M. and Rubin, A.B. (1989) FEBS Lett. 258, 27–31.
[22] Van Dorssen, R.J., Breton, J., Plijter, J.J., Satoh, K., Van Gorkom, H.J. and Amesz, J. (1987) Biochim. Biophys. Acta 893, 267–274.
[23] Sieckman, I., Brettel, K., Bock, C., Van der Est, A. and Stehlik, D. (1993) Biochemistry 32, 4842–4847.
[24] Den Blanken, H.J., Hoff, A.J., Jongenelis, A.P.J.M. and Diner, B.A. (1983) FEBS Lett. 157, 21–27.
[25] Van der Vos, R. and Hoff, A.J. (1992) in Research in Photosynthesis, Vol. I (Murata, N., ed.), pp. 215–218, Kluwer, Dordrecht, The Netherlands.
[26] Monotoya, G., (1993) presentation at the ESF workshop "Spectroscopy of the D1-D2 complex", Mülheim an der Ruhr, Germany.
[27] Angerhofer, A., Bernlocher, D. and Robert, B. (1993) Z. f. Phys. Chem. 180, 167–180.
[28] Ide, J.P., Klug, D.R., Kühlbrandt, W., Giorgi, L.B. and Parson, G. (1987) Biochim. Biophys. Acta 893, 349–364.
[29] Booth, P.J., Crystall, B., Ahmad I., Barber, J., Porter, G. and Klug, D. (1991) Biochemistry 30, 7573–7586.
[30] Schelvis, J.P.M., Van Noort, P.I., Aartsma, T.J. and Van Gorkom, H.J. (1994) Biochim. Biophys. Acta 1184, 242–250.
[31] Van Kan, P.J.M., Groot, M.L., Kwa, S.L.S., Dekker, J.P. and Van Grondelle, R. (1992) in The Photosynthetic Bacterial Reaction Center II (Breton, J. and Verméglio, A., eds.), pp. 411–420, Plenum Press, New York.
[32] Bowers, P.G. and Porter, G. (1967) Proc. R. Soc. A 296, 435–441.
[33] Chidsey, C.E.D., Takiff, L., Goldstein, R.A. and Boxer, S.G. (1985) Proc. Natl. Acad. Sci. USA 82, 6850–6854.
[34] Haberkorn, R., Michel-Beyerle, M.E. and Marcus, R.A. (1979) Proc. Natl. Acad. Sci. USA 76, 4185–4188.
[35] Ogrodnik, A., Volk, M., Letterer, R., Feick, R. and Michel-Beyerle, M.E. (1988) Biochim. Biophys. Acta 936, 361–371.
[36] Hoganson, C.W. and Babcock, G.T. (1989) Biochemistry 28, 1448–1454.
[37] Klimov, V.V., Dolan, E. and Ke, B. (1980) FEBS Lett. 112, 97–100.
[38] Durrant, J., Giorgi, L.B., Barber, J., Klug, D.R. and Porter, G. (1990) Biochim. Biophys. Acta 1017, 167–175.
[39] Goldstein, R.A. and Boxer, S.G. (1989) Biophys. J. 51, 937–946.